Supporting Information

Ratiometric SERS Detection of N_2H_4 by Porous Ag(I)-linked Waugh-type Polyoxometalate as Efficient Label-free Substrate

Jie Wang, Jia-Yuan Zhang, Wen-Jing Zhu, Bin Qi, Jun-Peng Wang, Guang-Gang Gao,* Lin-Lin Fan, and Hong Liu*

School of Materials Science and Engineering, *University of Jinan*, *Jinan*, *250022*, *China*.

* *Corresponding authors*.

E-mail: *mse_gaogg@ujn.edu.cn* (G.-G. Gao), *mse_liuh@ujn.edu.cn* (H. Liu).

Contents

concentrations of N_2H_4 (10^{-4}-1.0 mg/L) (b).

Fig. S9 The TEM image (a) and PXRD pattern (b) of **Ag_6MnMo_9** in the presence of 1.0 mg/L N_2H_4.

Fig. S10 Raman spectra of **Ag_6MnMo_9** at laser power (a) and sampling time (b). (c) A set of Raman spectra of **Ag_6MnMo_9** from 10 random positions. (d) The Raman intensity at 945 cm^{-1} from 10 random positions.

Fig. S11 (a) A set of SERS spectra of **Ag_6MnMo_9** exposed 10^{-3} mg/L N_2H_4 from 20 random positions. (b) The SERS intensity at 945 cm^{-1} from 20 random positions.

Fig. S12 The histogram of SERS signal at 945 cm^{-1} of three **Ag_6MnMo_9** SERS substrates exposed to 10^{-3} mg/L N_2H_4.

Fig. S13 TEM images of **Ag_6MnMo_9** before (a) and after (b) N_2H_4 treatment (inset of b: The HRTEM of **Ag_6MnMo_9** after N_2H_4 treatment). The overlay distribution of elements (c) and elemental mappings of Mo (d), Ag (e) and Mn (f).

Fig. S14 AgNPs size distribution for **Ag_6MnMo_9** after N_2H_4 treatment.

Fig. S15 PXRD patterns of **Ag_6MnMo_9** without and with the presence of N_2H_4.

Fig. S16 XPS survey spectra of **Ag_6MnMo_9** without and with the presence of N_2H_4.

Fig. S17 XPS analysis of **Ag_6MnMo_9** before and after reduction by N_2H_4 for O 1s.

Fig. S18 TEM images of **Ag_3MnMo_9** before (a) and after (b) N_2H_4 treatment. The overlay distribution of elements (c) and elemental mappings of Mo (d), Ag (e) and Mn (f) in **Ag_3MnMo_9**.

Fig. S19 (a) XPS survey spectra of **Ag_3MnMo_9** before and after reduction by N_2H_4; the core level XPS spectra for Mo 3d (b), Mn 2p (c) and Ag 3d (d).

Fig. S20 UV-vis absorbance spectra of **Ag_6MnMo_9** and its reduced state by reaction with N_2H_4.

Table S1 Crystal Data and Structure for complexes **Ag_6MnMo_9** and **Ag_3MnMo_9**.

Table S2 Raman and SERS vibrational frequencies (cm^{-1}) of **Ag_6MnMo_9**[a].

Table S3 Comparison of different methods for detecting N_2H_4.

Chemicals and materials

All reagents were purchased commercially and used without further purification. $(NH_4)_6[MnMo_9O_{32}]\cdot 8H_2O$ ($MnMo_9$) was prepared according to the literature method.[1] $AgNO_3$ (99%) and $MnSO_4\cdot H_2O$ (99%) were purchased from Macklin. $(NH_4)_6Mo_7O_{24}\cdot 4H_2O$ was purchased from Sigma-Aldrich. NH_4OH, Phenethylamine (PEA), triethylamine (TEA), N,N-Dimethylformamide (DMF), $(NH_4)_2S_2O_8$ (98%), 1,2,4-triazole (trz, 98%), acetonitrile, acetic acid and N_2H_4 were obtained from Alfa Aesar.

Characterization methods

The morphologies of the samples were studied on the ransmission electron microscopy (TEM, JEOL 2010, 200 kV). The powder X-ray diffraction (PXRD) patterns were performed on Rigaku/Max-2550 with Cu Kα radiation (λ = 1.7890 Å). The element distribution was measured by Energy dispersive spectrometer (EDS) on JEOL TEM. X-ray photoelectron spectroscopy (XPS) scans were carried on multifunctional imaging electron spectrometer (Thermo ESCALAB 250XI). The elemental analyses of H and N were conducted on a Vario EL III elemental analyzer, and those of Mo, Mn and Ag were analyzed on a Jarrel-AshJ-A1100 (ICP) atomic emission spectrometer. SERS testing was performed using a Raman spectrometer (Labramis, Horiba Jobbin Yvon, Paris, France). The wavelength was 532 nm. The laser power was 5 mW for all experiments. Spectra were collected with a 50-object lens for 4 s.

X-ray crystallography

Crystal data were collected on an Agilent Technology Eos Dual system with focusing multilayer mirror optics and a Cu Kα source of λ = 1.54184 Å. Empirical absorption corrections were applied to the intensities using the SADABS program. The structures were solved using the program SHELXS97 and refined with the program SHELXL-97. The positions of the metal atoms and their first coordination spheres were located from direct-methods. Other non-hydrogen atoms were found in alternating difference Fourier syntheses and least-squares refinement cycles. During the final cycles, except for some solvent molecules, all other non-hydrogen atoms were refined anisotropically. Hydrogen atoms were placed in calculated positions refined using idealized geometries and assigned fixed isotropic displacement parameters. CCDC number of 2086764 for **Ag_6MnMo_9** and 2097830 for **Ag_3MnMo_9**.

Supporting figures

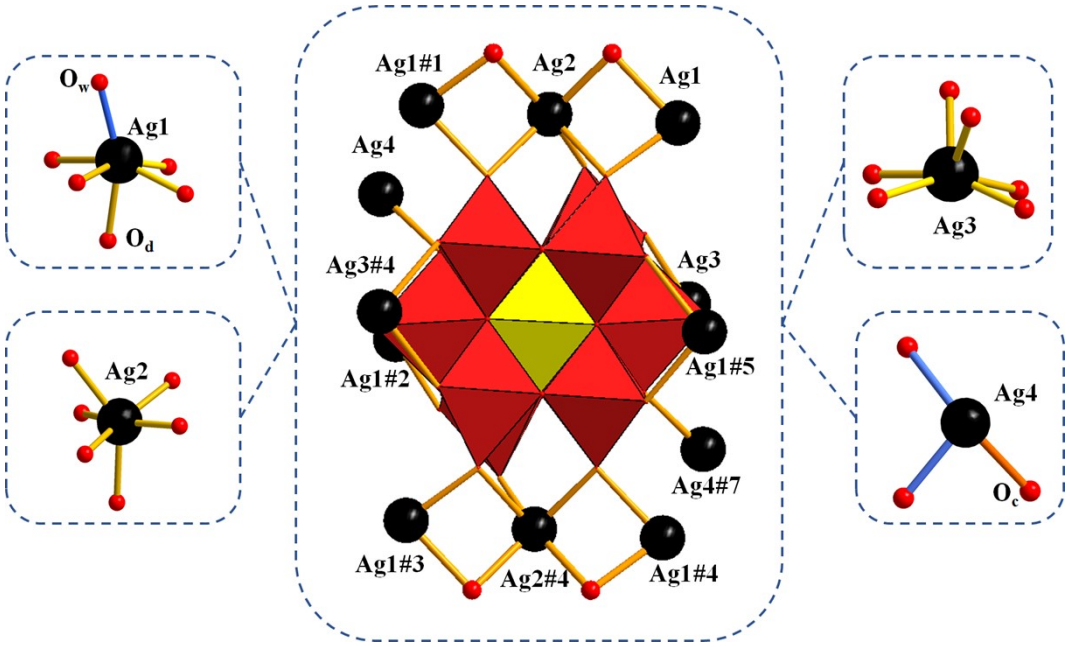

Fig. S1 Coordination environment of Ag^+ and $MnMo_9$ polyoxoanion. Symmetric code: #1 2-x, y, 1/2-z; #2 3/2-x, 1/2-y, -1/2+z; #3 1-x, y, 1/2-z; #4 -1+x, y, z; #5 -1/2+x, 1/2-y, 1-z; #6 -1/2+x, 1/2+y, z; #7 1-x, 1-y, 1/2+z.

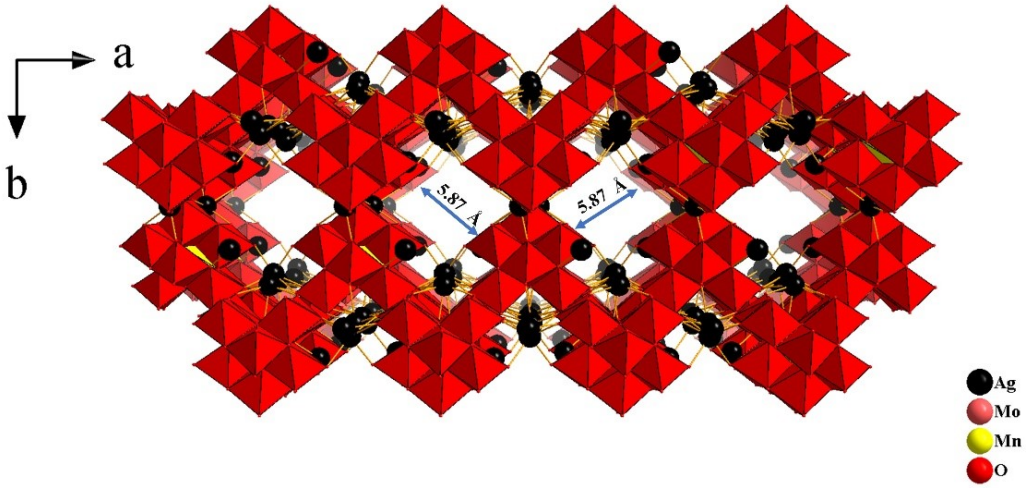

Fig. S2 Representation of 3D structure of **Ag_6MnMo_9** along axis *c*.

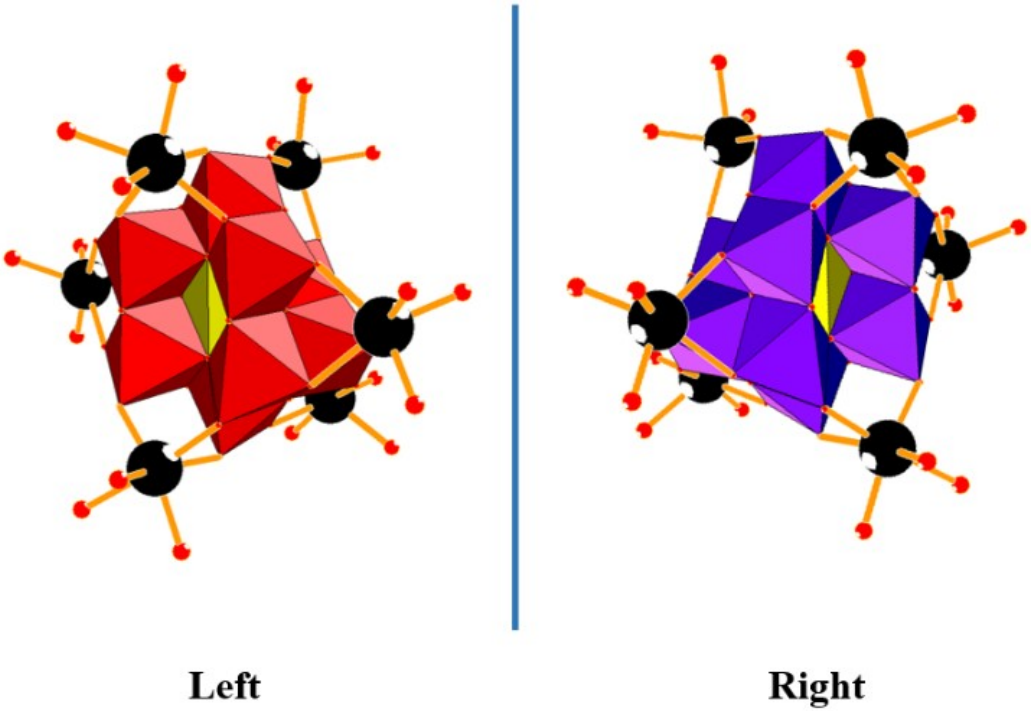

Fig. S3 Structures of left- and right- handed $MnMo_9$ polyoxoanions located in **Ag_3MnMo_9**.

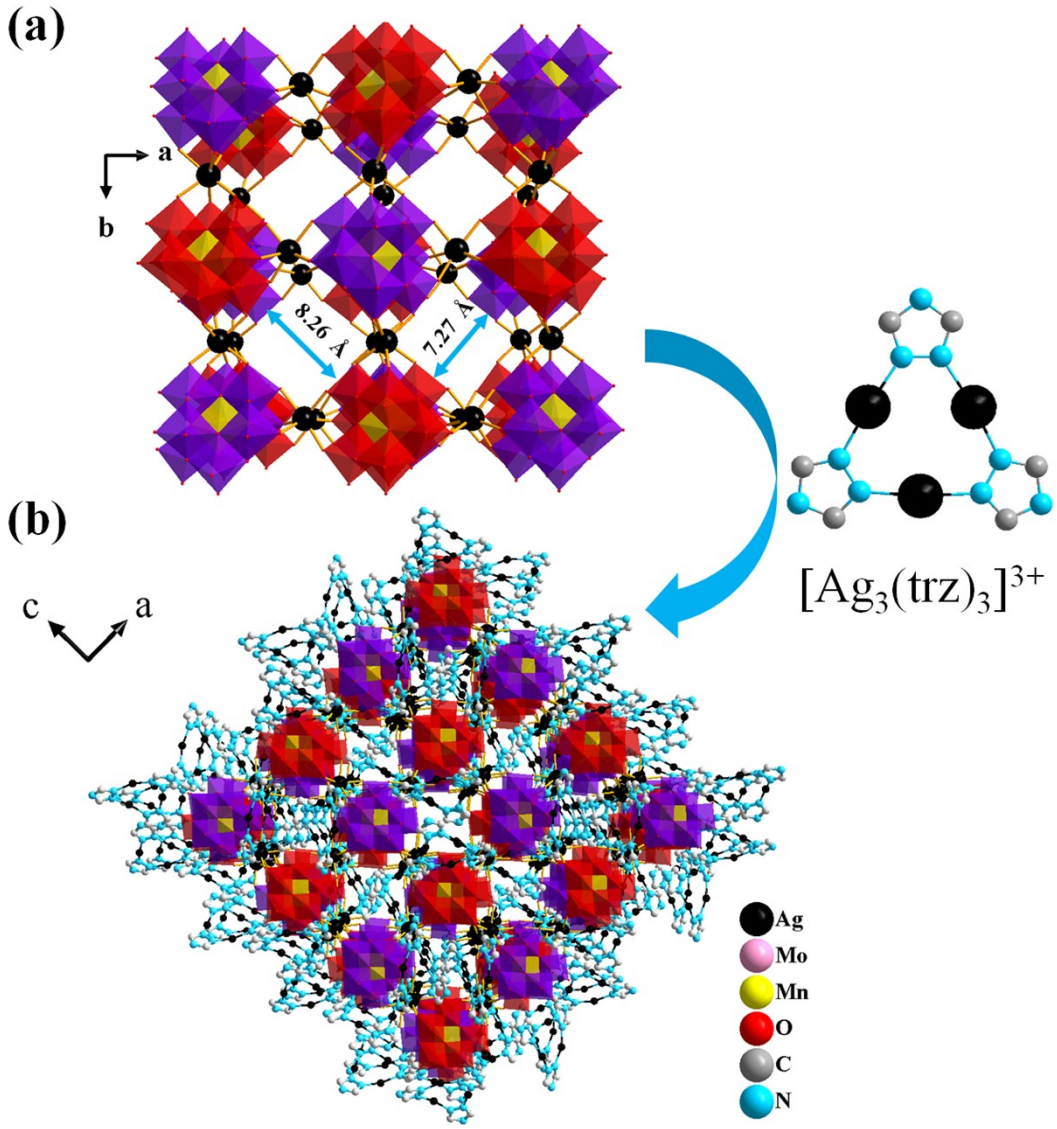

Fig. S4 (a) Representation of different chiral $[MnMo_9O_{32}]^{6-}$ polyoxoanions in **Ag_3MnMo_9**. (b) 3D framework of **Ag_3MnMo_9** filled with $[Ag_3(trz)_3]^{3+}$.

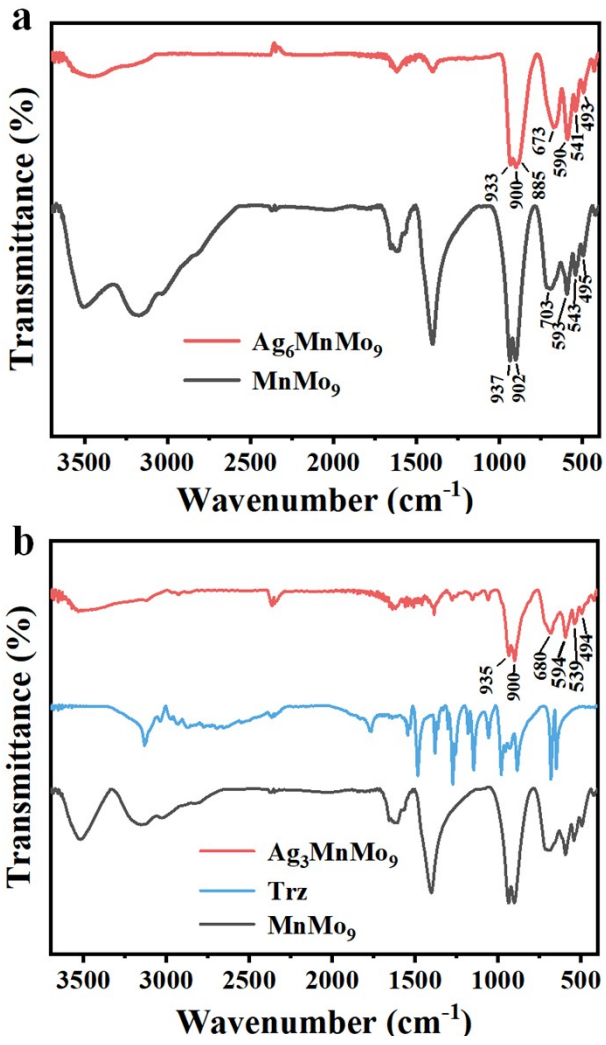

Fig. S5 Comparative FTIR curves for **Ag_6MnMo_9** and $MnMo_9$ (a) and **Ag_3MnMo_9**, $MnMo_9$ and trz (b).

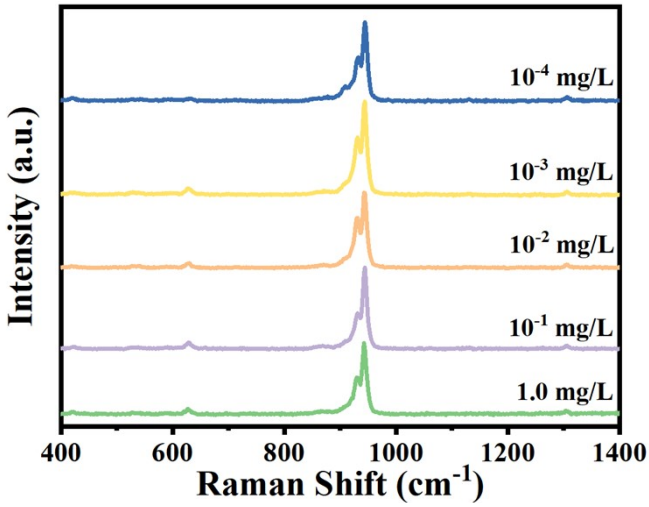

Fig. S6 (a) SERS spectra of **Ag_3MnMo_9** after reactions with different concentrations of N_2H_4 (10^{-4}-1.0 mg/L).

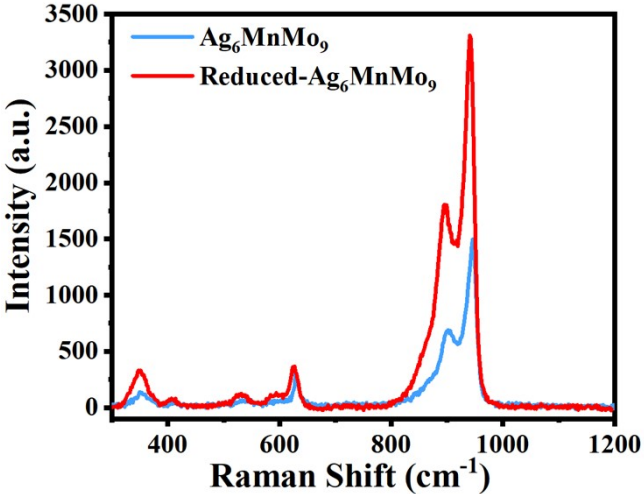

Fig. S7 The Raman and SERS spectra of **Ag_6MnMo_9** and **Ag_6MnMo_9** in the presence of 10^{-3} mg/L N_2H_4, respectively.

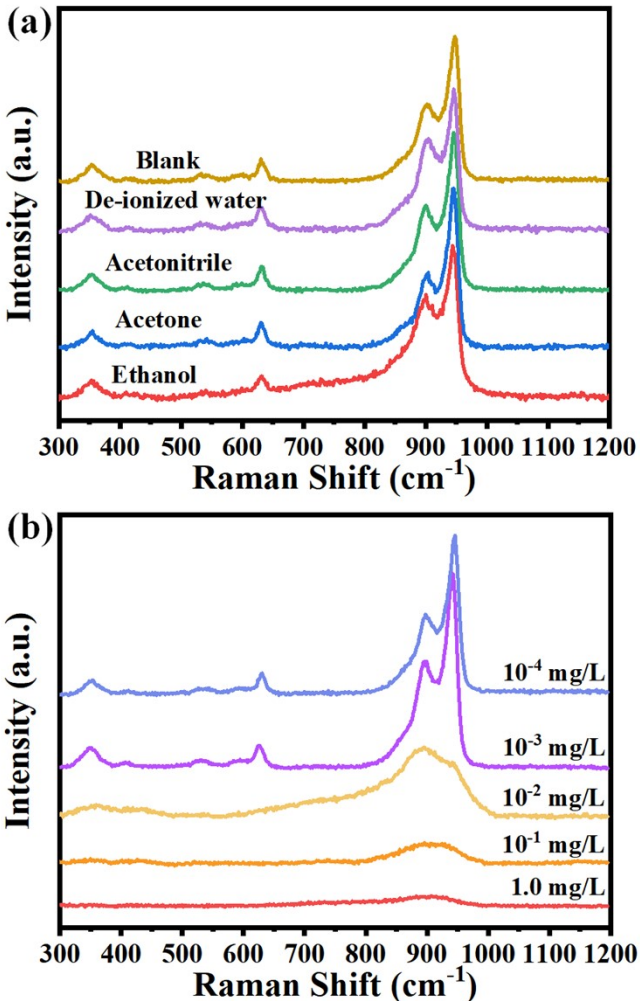

Fig. S8 SERS spectra of $\mathbf{Ag_6MnMo_9}$ in different solvents (a) and different concentrations of N_2H_4 (10^{-4}-1.0 mg/L) (b).

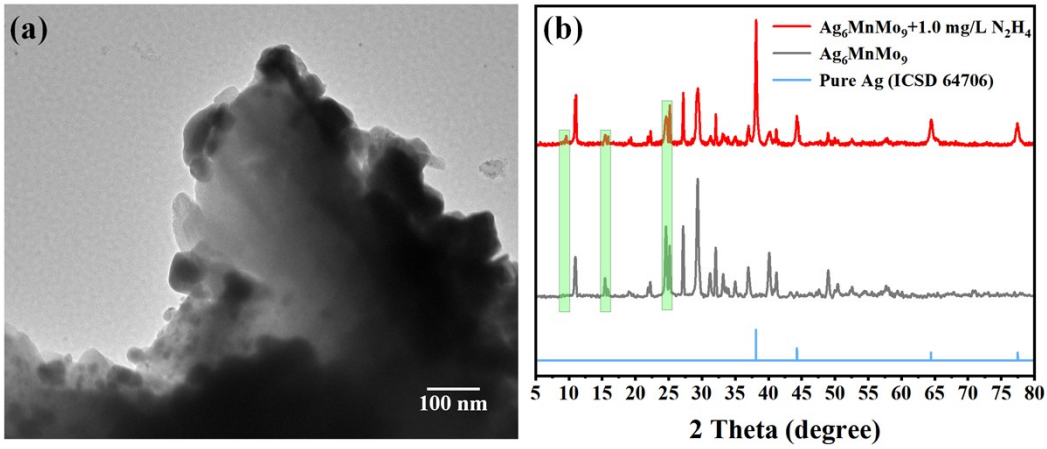

Fig. S9 The TEM image (a) and PXRD pattern (b) of **Ag_6MnMo_9** in the presence of 1.0 mg/L N_2H_4.

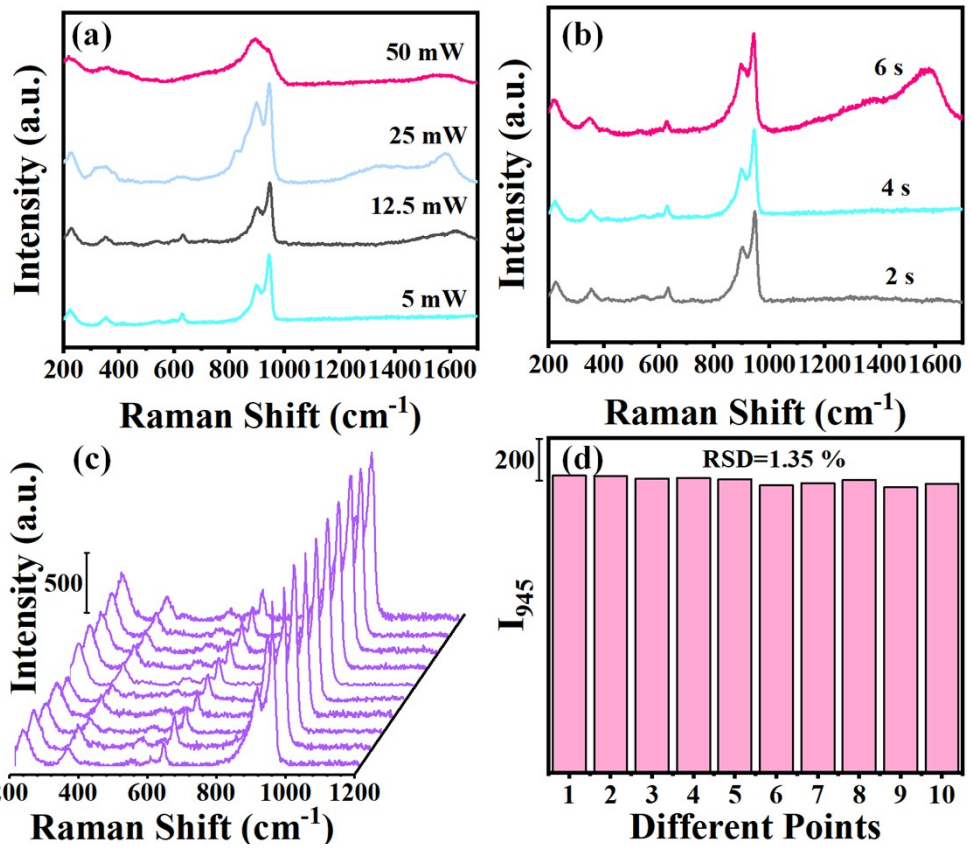

Fig. S10 Raman spectra of **Ag_6MnMo_9** at laser power (a) and sampling time (b). (c) A set of Raman spectra of **Ag_6MnMo_9** from 10 random positions. (d) The Raman intensity at 945 cm^{-1} from 10 random positions.

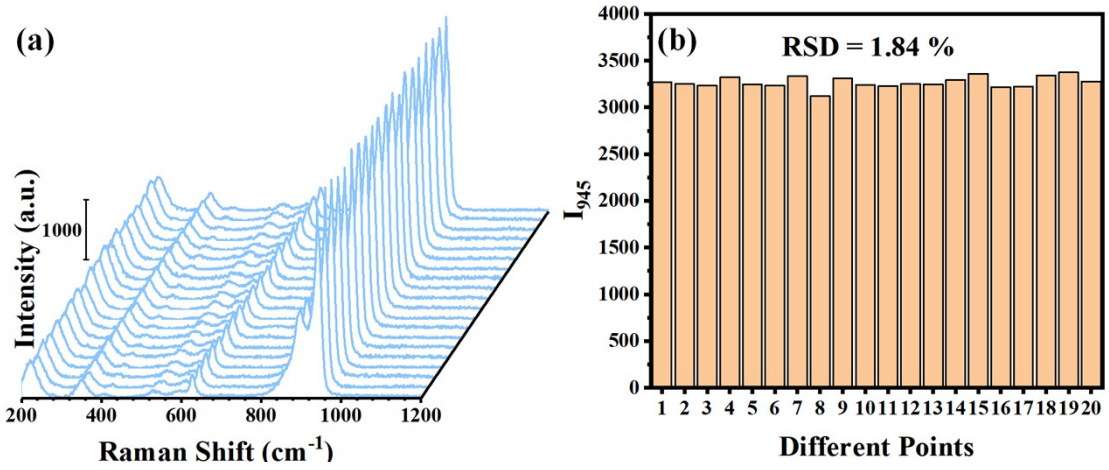

Fig. S11 (a) A set of SERS spectra of **Ag_6MnMo_9** exposed 10^{-3} mg/L N_2H_4 from 20 random positions. (b) The SERS intensity at 945 cm^{-1} from 20 random positions.

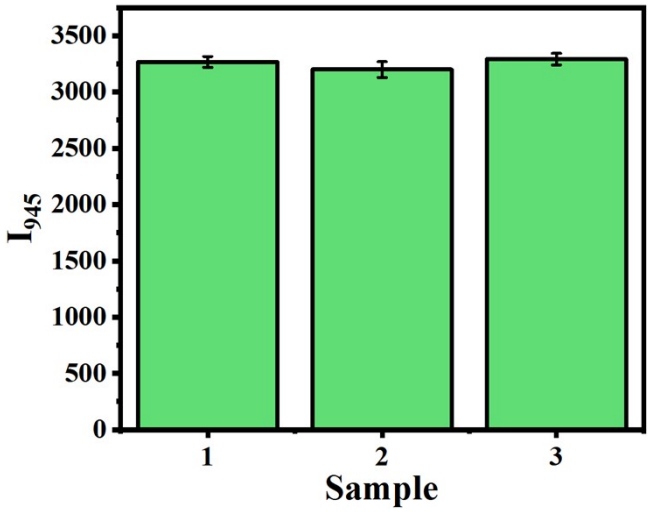

Fig. S12 The histogram of SERS signal at 945 cm^{-1} of three $\mathbf{Ag_6MnMo_9}$ SERS substrates exposed to 10^{-3} mg/L N_2H_4.

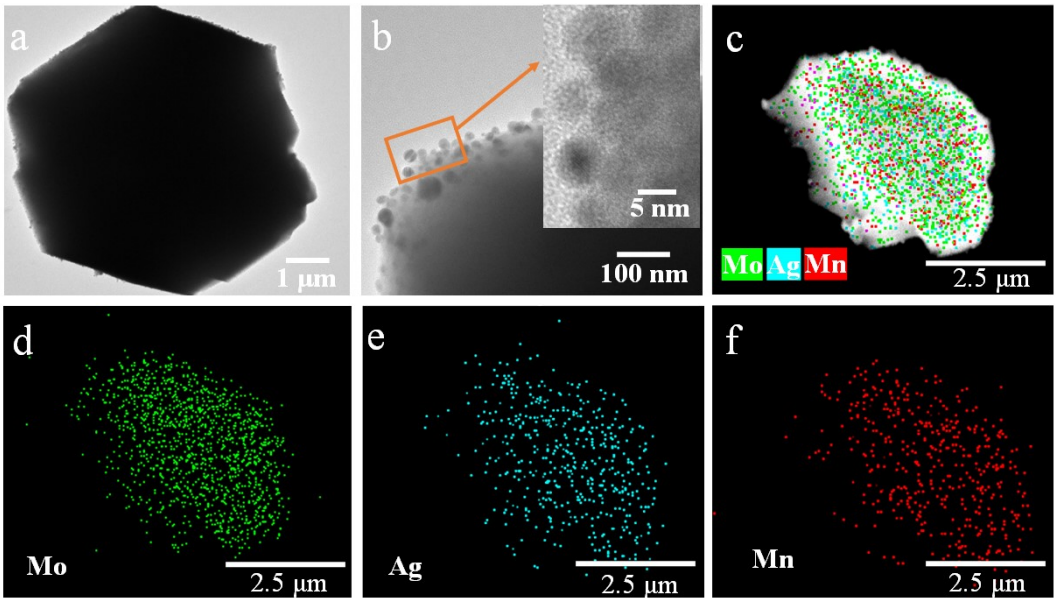

Fig. S13 TEM images of **Ag_6MnMo_9** before (a) and after (b) N_2H_4 treatment (inset of b: The HRTEM of **Ag_6MnMo_9** after N_2H_4 treatment). The overlay distribution of elements (c) and elemental mappings of Mo (d), Ag (e) and Mn (f).

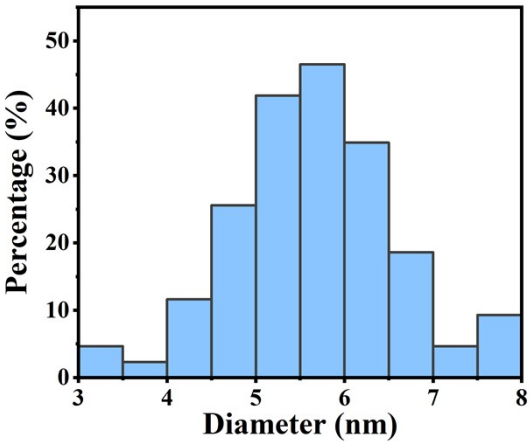

Fig. S14 AgNPs size distribution for **Ag_6MnMo_9** after N_2H_4 treatment.

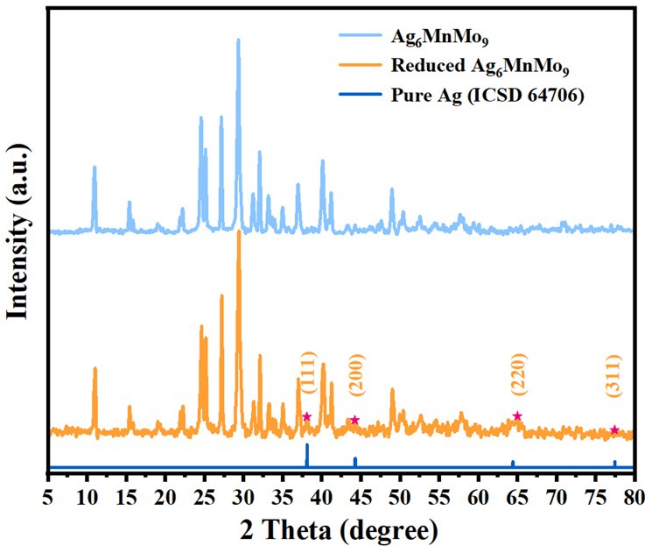

Fig. S15 PXRD patterns of **Ag_6MnMo_9** without and with the presence of N_2H_4.

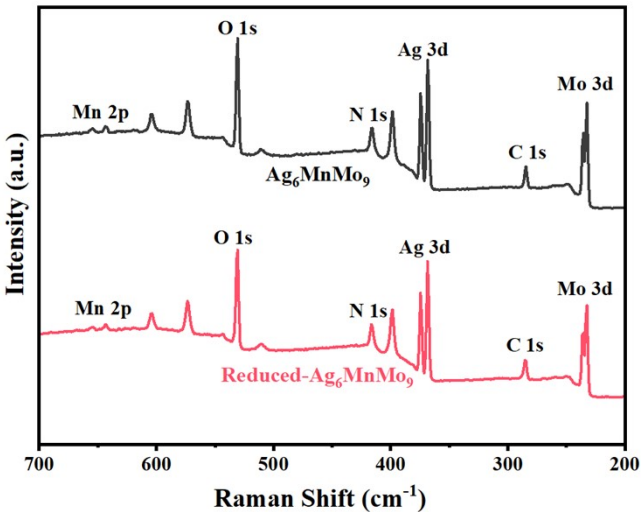

Fig.S16 XPS survey spectra of **Ag_6MnMo_9** without and with the presence of N_2H_4.

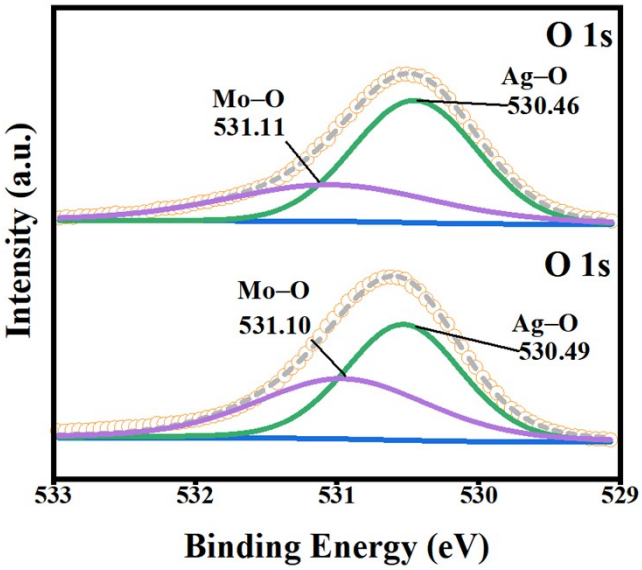

Fig. S17 XPS analysis of **Ag_6MnMo_9** before and after reduction by N_2H_4 for O 1s.

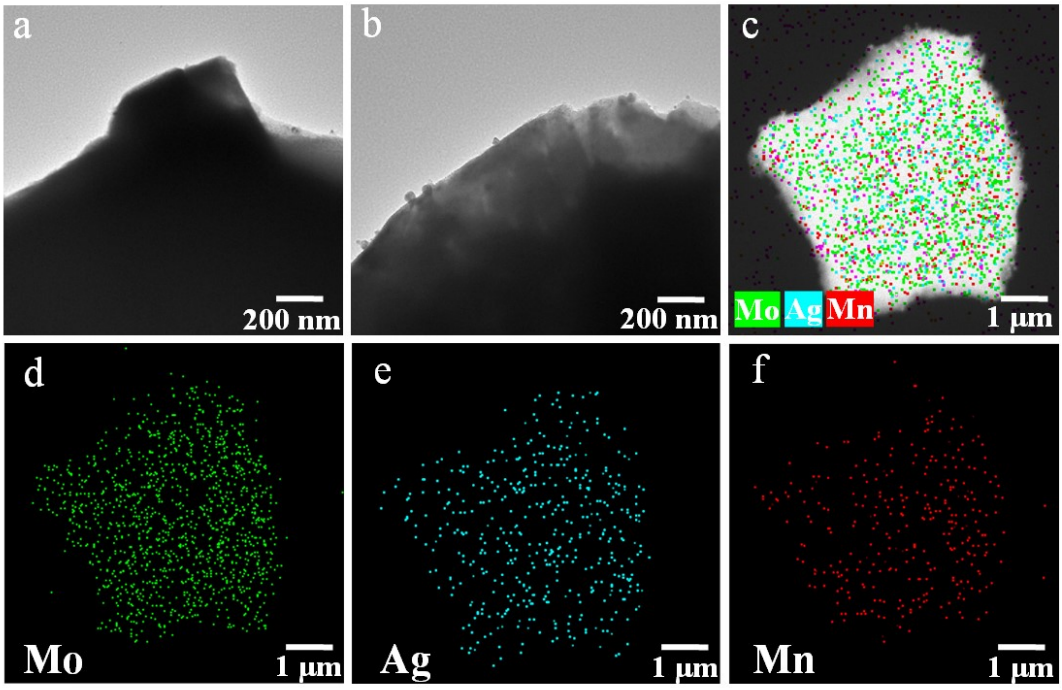

Fig.S18 TEM images of **Ag_3MnMo_9** before (a) and after (b) N_2H_4 treatment. The overlay distribution of elements (c) and Elemental mappings of Mo (d), Ag (e) and Mn (f) in **Ag_3MnMo_9**.

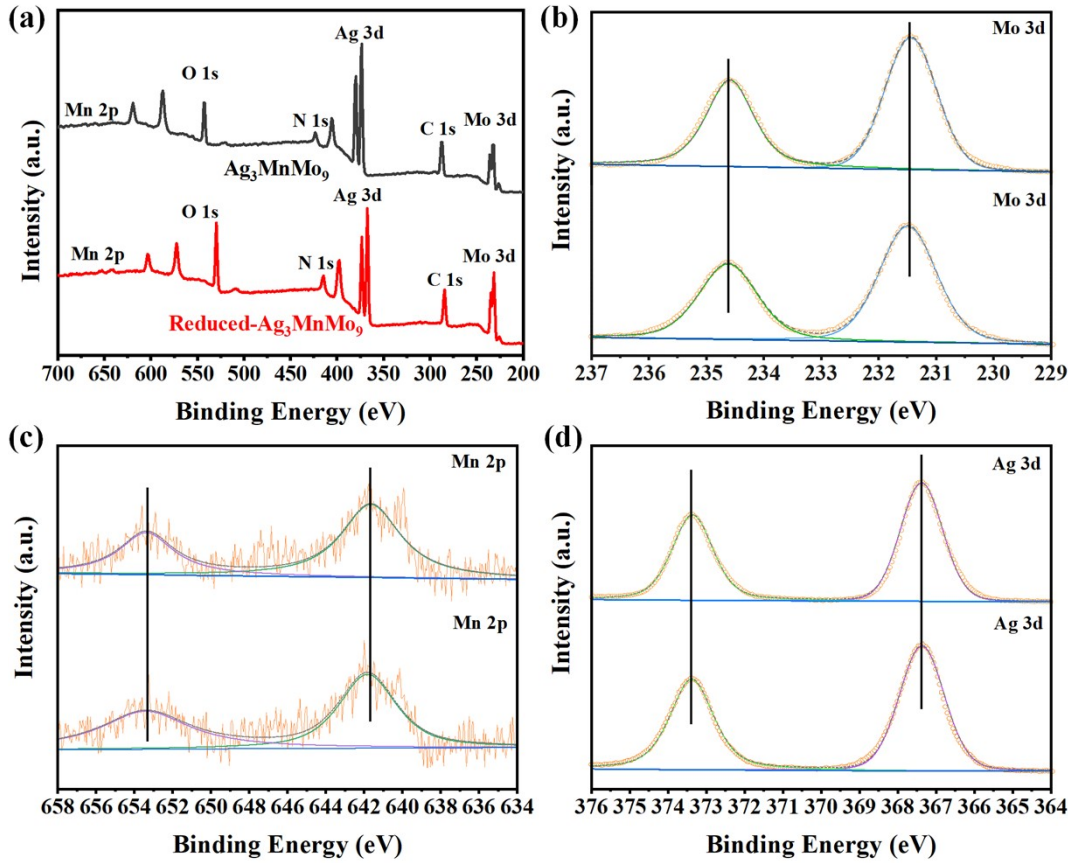

Fig. S19 XPS spectra of survey (a), Mo 3d (b), Mn 2p (c) and Ag 3d (d) of **Ag_3MnMo_9**.

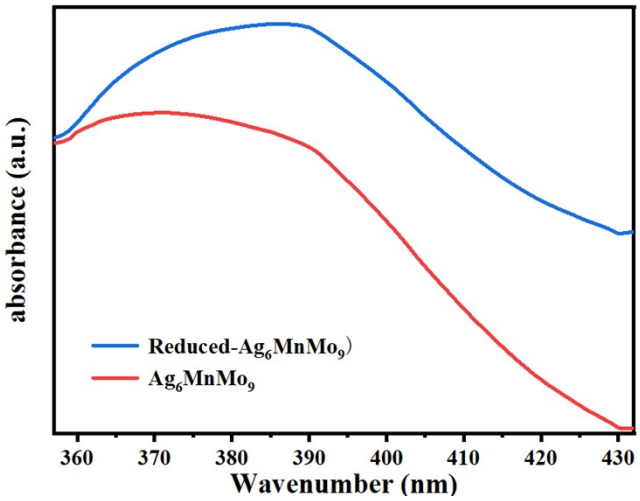

Fig.S20 UV-vis absorbance spectra of **Ag_6MnMo_9** and its reduced state by reaction with N_2H_4.

Table S1 Crystal Data and Structure for complexes **Ag_6MnMo_9** and **Ag_3MnMo_9**.

Compound	**Ag_6MnMo_9**	**Ag_3MnMo_9**
Empirical formula	$H_4O_{36}Ag_6Mn_1Mo_9$	$H_{24}C_6H_{24}N_9O_{41}Ag_6Mn_1Mo_9$
Formula weight	2145.62	2427.77
T (K)	293(2)	293(2)
Space group	$C222_1$	$Pa\bar{3}$
Crystal system	Orthorhombic	Cubic
a / Å	10.9514(9)	21.4897(2)
b / Å	24.5879(17)	21.4897(2)
c / Å	15.3537(10)	21.4897(2)
a / °	90)	90
β / °	90	90
γ / °	90	90
V / Å^3	4134.3(5)	9924.1(3)
Z	4	8
D_c / g cm^{-3}	3.441	3.218
F (000)	3892.0	8832.0
Reflns collected / unique	6190 / 2919	26361 / 2924
$R_{(int)}$	0.0444	0.0619
Goodness-of-fit on F^2	1.047	0.953
final R indices [I>2σ(I)]	R_1[a] = 0.0791 wR_2[b] = 0.2013	R_1[a] = 0.0294 wR_2[b] = 0.0701
R indices (All data)	R_1[a] = 0.0803 wR_2[b] = 0.2026	R_1[a] = 0.0332 wR_2[b] = 0.0721
CCDC	2086764	2097830

[a] $R_1 = \sum||F_o| - |F_c||/\sum|F_o\}|$. [b] $wR_2 = \{\sum[w(F_o^2 - F_c^2)^2]/\sum[w(F_o^2)^2]\}^{1/2}$.

Table S2. Raman and SERS vibrational frequencies (cm^{-1}) of $\mathbf{Ag_6MnMo_9}$[a].

SERS	Raman	Vibrational assignments
945	945	υ Mo–O_d
898	898	υ Mo–O_b–Mo
	630	υ Mn–O_a–Mo
531	534	υ Mo–O_c–Mo
347	353	δ Mo–O_c–Mo

[a] υ, stretching; δ, bending.

Table S3. Comparison of different methods for detecting N_2H_4.

Method	Linear range	Limit of detection	References
fluorometry	0.75 – 1.5 μM	204 nM	2
fluorometry	0 – 15 μM	0.16 μM	3
fluorometry	0 – 75 μM	82 nM	4
fluorometry	0 – 15 μM	0.075 μM	5
fluorometry	0 – 6 μM	90 nM	6
fluorometry	0 – 500 μM	0.3 μM	7
fluorometry	0 – 50 μM	81.8 nM	8
chromatography	0 – 0.06 mM	0.013 mM	9
chromatography	0.05 – 1 μM	9.6 nM	10
SERS	10^{-10} – 10^{-9} M	85 pM	11
SERS	10^{-9} – 10^{-7} M	38 pM	12
SERS	10^{-3} – 10^{-10} mg/L	40 pg/L (2 pM)	**This work**

References

1 L. C. W. Baker, T. J. R. Weakley, *J. Inorg. Nucl. Chem.* 1966, **28**, 447-454.

2 S. K. Samanta, K. Maiti, S. S. Ali, U. N. Guria, A. Ghosh, P. Datta, A. K. Mahapatra, *Dyes Pigm.*, 2020, **173**, 107997.

3 J. P. Wang, C. R. Wang, S. Jiang, W. Y. Ma, B. Xu, L. J. Liu, W. J. Tian, *J. Mater. Chem.* C, 2022, **10**, 2807-2813.

4 Y. Wang, X. L. Xue, Q. Zhang, K. P. Wang, S. J. Chen, L. S. Tang, Z. Q. Hu, *Spectrochim. Acta A Mol. Biomol. Spectrosc.*, 2022, **279**, 121406.

5 L. Y. Wang, S. Q. Xin, F. R. Xie, X. G. Ran, H. Tang, D. R. Cao, *J. Mater. Chem.* C, 2022, **10**, 14605-14615.

6 Q. Q. Lai, S. F. Si, T. Y. Qin, B. J. Li, H. X. Wu, B. Liu, H. H. Xu, C. Zhao, *Sens. Actuators B Chem.*, 2020, **307**, 127640.

7 C. H. Zeng, Z. Y. Xu, C. Song, T. Y. Qin, T. H. Jia, C. Zhao, L. Wang, B. Liu, X. J. Peng, *J. Hazard. Mater.*, 2023, **445**, 130415.

8 S. Q. Zhang, Y. Xie, L. Q. Yan, *Acta A Mol. Biomol. Spectrosc.*, 2020, **230**, 118028.

9 R. Sharma, S. H. Jung, H. I. Lee, *ACS Appl. Polym. Mater.*, 2021, **3**, 6632-6641.

10 Y. Zhang, Y. Zhang, D. Zhang, S. D. Li, C. Jiang, Y. Su, *Sens. Actuators B Chem.*, 2019, **285**, 607-616

11 X. Gu, J. P. Camden, *Anal. Chem.*, 2015, **87**, 6460-6464.

12 G. D. Xu, N. Guo, Q. J. Zhang, T. T. Wang, P. Song, L. X. Xia, *J. Hazard. Mater.*, 2022, **424**, 127303.